Editors' Suggestion

Observation of Interatomic Coulombic Decay Induced by Double Excitation of Helium in Nanodroplets

B. Bastian,[1] J. D. Asmussen,[2] L. Ben Ltaief,[2] H. B. Pedersen,[2] K. Sishodia,[3] S. De,[3] S. R. Krishnan,[3] C. Medina,[5] N. Pal,[6] R. Richter,[6] N. Sisourat,[7] and M. Mudrich[2,*]

[1]*Wilhelm Ostwald Institute for Physical and Theoretical Chemistry, Leipzig University, Linnéstraße 2, 04103 Leipzig, Germany*
[2]*Department of Physics and Astronomy, Aarhus University, 8000 Aarhus C, Denmark*
[3]*Quantum Center of Excellence for Diamond and Emergent Materials and Department of Physics, Indian Institute of Technology Madras, Chennai 600036, India*
[5]*Max Planck Institute for Nuclear Physics, Saupfercheckweg 1, 69117 Heidelberg, Germany*
[6]*Elettra-Sincrotrone Trieste, 34149 Basovizza, Trieste, Italy*
[7]*Sorbonne Université, CNRS, Laboratoire de Chimie Physique Matière et Rayonnement, UMR 7614, F-75005 Paris, France*

(Received 26 October 2023; accepted 25 April 2024; published 3 June 2024)

Interatomic Coulombic decay (ICD) plays a crucial role in weakly bound complexes exposed to intense or high-energy radiation. So far, neutral or ionic atoms or molecules have been prepared in singly excited electron or hole states that can transfer energy to neighboring centers and cause ionization and radiation damage. Here we demonstrate that a doubly excited atom, despite its extremely short lifetime, can decay by ICD; evidenced by high-resolution photoelectron spectra of He nanodroplets excited to the $2s2p+$ state. We find that ICD proceeds by relaxation into excited He^*He^+ atom-pair states, in agreement with calculations. The ability of inducing ICD by resonant excitation far above the single-ionization threshold opens opportunities for controlling radiation damage to a high degree of element specificity and spectral selectivity.

DOI: 10.1103/PhysRevLett.132.233001

Highly excited atoms and molecules embedded in an environment can efficiently decay by exchange of energy or charge with an atom or molecule in their environment through interatomic (intermolecular) electronic correlation. These processes, termed interatomic (intermolecular) Coulombic decay (ICD), cause ionization of the neighboring center, thereby quenching concurrent decay processes [1–6]. Since the prediction of ICD as an efficient decay process of clusters with an excited intermediate-shell electron [7], a variety of related processes have been discovered involving both neutral and ionic species. The general relevance of ICD has been established, with implications for radiation damage of biological matter [8–12].

A special class of electronic excitations is given by doubly excited states of atoms and molecules that manifest themselves as resonances in photoionization (PI) spectra [13–18]. A paradigm system is the helium atom (He^{**}) where the two electrons occupy discrete excited states within the photoionization continuum. Excitation into these states leads to the same final state via two pathways; direct PI and autoionization (AI) of the He^{**} both form a He^+ and an electron. Quantum interference of the two indistinguishable paths causes the well-known asymmetric Fano line shape [19]. The first series of these Fano resonances appears around 60 eV photon energy [20–22]. When a second ground state He atom is placed next to the He^{**}, an additional nonlocal autoionization process may open up—ICD; see Fig. 1 for a schematic representation. The decay of isolated He^{**} atoms (upper pathway) has been studied in detail both theoretically and experimentally; the lowest optically accessible doubly excited state, $2s2p+$, decays by AI in only 17.5 fs [20,21]. Decay of He^{**} by ICD (lower path) has only been considered theoretically for the diatomic system $He^{**}Ne$ [3]. In this process, one of the two electrons decays to the ground state and the resulting energy is transferred to a neighboring atom which in turn is ionized. The decay by fluorescence emission only becomes a relevant concurrent decay path for higher

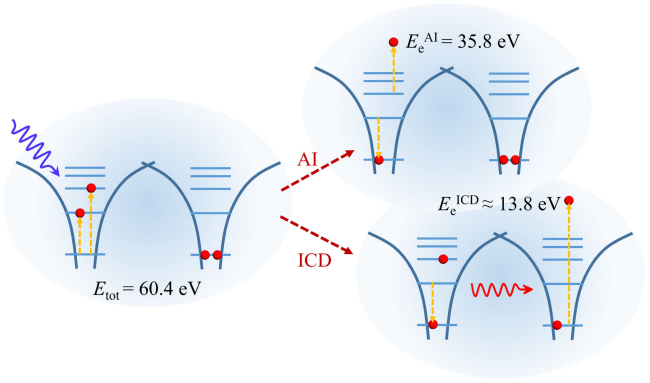

FIG. 1. Schematics of a pair of He atoms where one is in a doubly excited state that can decay by intraatomic autoionization or by interatomic Coulombic decay.

states and is therefore disregarded here. A related resonant ICD process which has been experimentally studied in neon clusters is initiated by excitation of a single $2s$ inner valence electron to a Rydberg state [23–26]; ICD then proceeds by relaxation of a Ne $2p$ valence electron to fill the $2s$ hole whereas the excited Rydberg electron does not participate in the ICD process. In contrast, here two electrons are excited from the ground state in a correlated fashion, one of which decays again to drive the ICD process. In "resonant-Auger-induced ICD" an inner valence shell-excited ion is created by intraatomic resonant Auger decay and ICD proceeds subsequently from this state interacting with a neutral neighbor [27–30]. This process is similar to the originally proposed ICD [7] (a single inner valence hole state triggers ICD) but clearly distinct from the ICD mechanism reported here.

ICD of doubly excited atoms is expected to be particularly efficient because these states are more sensitive to perturbations by neighboring atoms than those where only a single electron is excited [3]. In a more complex environment, which has not been considered until now, this type of ICD may be even faster; generally the ICD rate steeply rises for decreasing interatomic distance between the excited and the neighboring atom and it scales approximately proportionally to the number of neighbors [7,31].

Here we present a combined experimental and theoretical study of ICD of doubly excited He atoms in He nanodroplets. He nanodroplets have proven to be particularly well suited test beds for exploring ICD processes due to the simple electronic structure of the He atom which makes electron spectra easy to interpret and theoretical calculations tractable [32–40]. Double-excitation spectra of He nanodroplets feature Fano profiles with similarly asymmetric shape as the atomic lines. However, the droplet profiles are blueshifted and significantly broadened due to repulsive interaction between the excited electrons (as well as He^* states) and the surrounding He environment [41].

In this work we use two different techniques to measure photoelectron spectra: (i) A velocity-map imaging (VMI) spectrometer located at the synchrotron radiation source ASTRID2 at Aarhus University allows us to detect electrons and ions in coincidence [42]. (ii) A hemispherical electron analyzer (HEA) used at the Gasphase beamline of Elettra synchrotron in Trieste (model VG 220i mounted at the magic angle) allows us to measure high-resolution electron spectra. With the VMI spectrometer we detect the full distribution of electron energies E_e at photon energies in the range $h\nu = 58$–63 eV. In both setups, background and foreground data were measured intermittently using a chopper wheel that periodically blocks and unblocks the droplet beam.

To compute the total and partial decay widths of the $\mathrm{He}(2s2p) - \mathrm{He}(1s^2)$ $^1\Sigma_u$ and $^1\Pi_u$ states, we used the R-matrix method [43] as implemented in the UKRmol+ package [44] according to the details in the Supplemental Material Sec. I [45].

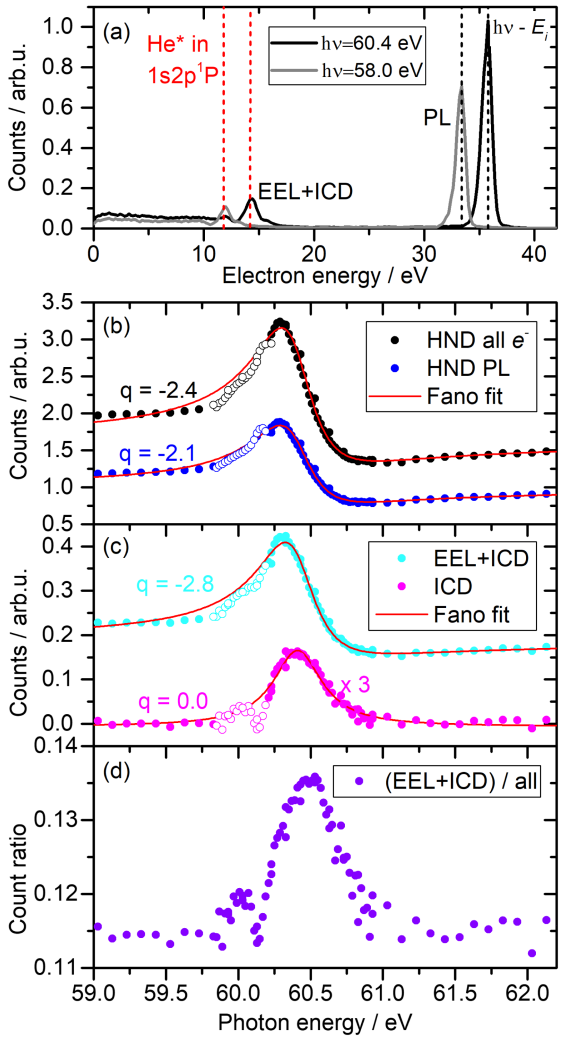

FIG. 2. Photoionization spectra of He nanodroplets ($\langle N \rangle \approx 4.3 \times 10^4$ He atoms per droplet) around the $2s2p+$ Fano resonance. (a) Photoelectron spectra recorded at $h\nu = 58$ and 60.4 eV using the VMI spectrometer. (b) Yield of direct photoelectrons and total electrons as a function of photon energy. (c) Yield of electrons subjected to energy loss due to inelastic scattering or ICD. (d) The ratio of energy loss to total electrons features a pronounced maximum indicating ICD at the resonance. For fits of the Fano profile in (b) and (c), only full circles were considered to exclude the sharp helium atomic line due to the atomic component in the droplet beam.

The electron spectra inferred from the VMI measurements contain two prominent features, see Fig. 2(a). A sharp peak at $E_e = h\nu - E_i$ electron kinetic energy, denoted as photoline (PL), is due to direct PI and AI which are indistinguishable processes. Here, $E_i = 24.59$ eV is the ionization energy of He. The small peak around $E_e = 15$ eV results mainly from electron energy loss by inelastic scattering (EEL) of the outgoing photoelectron at He atoms in the nanodroplet surrounding the photoion, according to the reaction [60]

$$\mathrm{He}_N + h\nu \rightarrow \mathrm{He}^+\mathrm{He}_{N-1} + e^-_{\mathrm{PL}} \rightarrow \mathrm{He}^+\mathrm{He}^*\mathrm{He}_{N-2} + e^-_{\mathrm{EEL}}.$$

In addition, ICD may contribute to this feature,

$$\mathrm{He}_N + h\nu \rightarrow \mathrm{He}^{**}\mathrm{He}_{N-1} \rightarrow \mathrm{He}^*\mathrm{He}^+\mathrm{He}_{N-2} + e^-_{\mathrm{ICD}}.$$

As the two reactions yield the same final state up to different $1snℓ$ levels of He^*, they are hard to distinguish in the electron spectra; see also Supplemental Material Fig. S1 [45]. However, ICD can only occur when the photon energy is tuned to a He^{**} resonance, while the inelastic scattering cross section is rather constant across the resonance such that the ratio of inelastically scattered to total electrons stays constant. Thus, we identify the ICD contribution by analyzing the yields of EEL + ICD electrons and total electrons as a function of photon energy $h\nu$. For each value of $h\nu$, the electron counts as a function of electron energy loss $E_l = h\nu - E_i - E_e$ are integrated from −2 to 2 eV for the photoelectrons, from 18 to 23 eV for the EEL + ICD electrons, and over the full range to obtain the total electron yield.

Figure 2(b) shows the yield of electrons emitted from He nanodroplets by PI and AI and 2(c) shows the yield of EEL + ICD electrons. The ratio of the two signals, shown in 2(d), reflects the probability of forming He^*; it features a maximum at $h\nu = 60.41 \pm 0.01$ eV, coinciding with the resonance energy that lies in the falling edge of the Fano profile. The relative contribution to this feature from electron-He inelastic scattering is not expected to significantly vary in the narrow tuning range $h\nu = 60$–61 eV around the He^{**} double excitation [54]. The resonant increase of the ratio compared to its average for off-resonant photon energies $h\nu < 59.9$ eV is therefore attributed to ICD. From the difference to the off-resonant ratio, we estimate the ICD electron yield shown in Fig. 2(c), see Supplemental Material Eq. (2) [45]. Interestingly, the spectral line shapes in Figs. 2(b) and 2(c) clearly differ from one another. Fits of the standard Fano profile [21,41] to the data (solid lines) result in an asymmetry parameter (or Fano parameter) $q = -2.13 \pm 0.05$ for the photoline and $q = -2.36 \pm 0.07$ for all electrons. The latter coincides with a previous measurement of all emitted electrons (mostly photoelectrons) [41] and comes close to the value for the atomic Fano profile ($q = -2.77$, [21]). For the EEL + ICD profile we find a similar value $q = -2.8 \pm 0.1$, while the ICD profile yields $q = 0.00 \pm 0.02$. Note that for $q = 0$ the Fano resonance profile is identical to the Breit-Wigner or Lorentzian formula for resonant excitation of a two-level system. The ICD signal is expected to follow the latter resonance curve because ICD can only occur for the one path involving He^{**} excitation, whereas the path of direct photoionization cannot lead to ICD. Symmetrically broadened ICD lines were previously observed for inner-valence-shell excited rare-gas dimers and clusters [61].

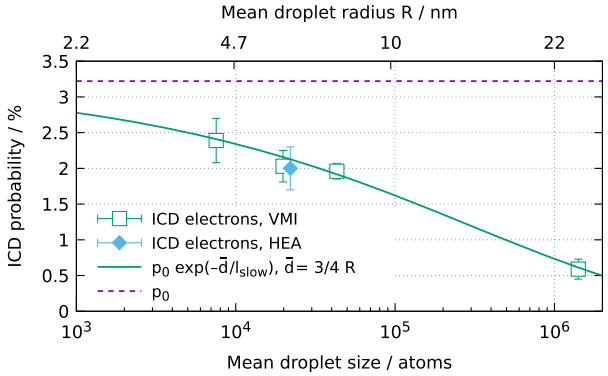

FIG. 3. Probabilities for the detection of ICD electrons relative to the total number of electrons as a function of average droplet size. The HEA point is computed as a product of the ICD to EEL + ICD ratio and the EEL + ICD probability for VMI data at a comparable average droplet size. The VMI data are fitted with a simple model to estimate the nascent ICD probability p_0.

VMI measurements at different expansion temperatures allow us to analyze ICD probabilities relative to total electrons as a function of droplet size [see Eq. (3), Sec. III, and Table I in the Supplemental Material [45]]. As ICD mostly occurs between nearest neighbors, no pronounced size dependence is expected in the studied range of droplet sizes; the apparent drop of the ICD probability in Fig. 3 for large droplets is attributed to the trapping of slow ICD electrons in bubbles that remain transiently bound to large droplets [55]. To quantify this effect, we assume a simple model, $p_{\mathrm{ICD}} = p_0 \exp(-\bar{d}/l_{\mathrm{slow}})$, where $\bar{d}$ is the mean distance of the ICD electron to the droplet surface [see Supplemental Material Eqs. (9)–(12) [45]] and l_{slow} is a mean free path. The fit to the data, shown as a solid red line in Fig. 3, yields $l_{\mathrm{slow}} = (11.1 \pm 1.1)$ nm and $p_0 = (3.2 \pm 0.2)\%$ as the nascent ICD probability inside the droplet. This gives an ICD decay time of ≈ 530 fs; see Supplemental Material Sec. IX [45]. Extrapolation to larger droplets shows that only one per thousand ICD electrons will be ejected out of a droplet of radius 100 nm which roughly matches the photoelectron trapping range of 150 nm for 15 eV electrons obtained from simulations, see the supplemental material of [56]. ICD and electron impact excitation probabilities for total electrons and electron-ion coincidences with He_n^+ ($n = 1, 2, 3$) as a function of droplet size are presented in Supplemental Material Sec. VI [45].

Our theoretical computations give a rough estimate of the ICD probability in competition with AI in the $\mathrm{He}^{**}\mathrm{He}$ system for the $^1\Sigma_u^+$ and $^1\Pi_g$ doubly excited states at five different pair distances r from 2.1 to 3.2 Å, respectively. As detailed in Supplemental Material Sec. VIII [45], we fit the average probability with an exponential function $p(r)$ and weight it with the pair-distance distribution function $g(r)$ [57,58] to obtain the overall ICD probability relative to the total ionization rate in the He droplet environment

$$p_0^{\text{theory}} = f_{\text{res}} \int p(r) g(r) \mathrm{d}r = (1.6 \pm 1.4)\%,$$

where $f_{\text{res}} = 0.51 \pm 0.03$ is the fraction of double excitation relative to total ionization at the resonance energy $E_r = 60.4$ eV, inferred from fits of the Fano profile (see Supplemental Material Sec. VIII [45]). The theoretical estimate is based on calculations for a helium dimer. Many-body effects of the surrounding helium atoms are therefore neglected which may explain the difference to the somewhat larger experimental value. Increased ICD to AI ratios are expected for higher-lying doubly excited states but preliminary results in Supplemental Material Figs. S3(e) and S3(f) [45] cannot discern the expected resonance in the EEL + ICD to PL ratio from the noise level.

To obtain more detailed insights into the ICD process we recorded high-resolution electron spectra of the EEL + ICD feature using the HEA. Figure 4(a) shows the average of 39 spectra recorded in the range $h\nu = 58.4$–62.2 eV (black circles) and a spectrum on resonance ($h\nu = 60.5$ eV, green triangles). Certain regions of the spectrum around 19 and 22.5 eV are clearly enhanced on resonance. This is confirmed by multipeak fits consisting of the sum of 8 Gaussians to account for various final states populated either by impact excitation by the photoelectron or by ICD. The peak widths, except that for the $1s2s(^3\mathrm{S})$ state, and the positions of the three Gaussian functions within the dominant $1s2p$ peak were fixed to fit the spectra for each energy, with their values determined from the well-converged fit of the average spectrum [individual peaks and fit residuals are shown in Supplemental Material Fig. S3(a) [45]]. For each state and photon energy, the (EEL + ICD)-to-total-electron ratio in Fig. S3(b) of [45] is computed to estimate the ICD fraction and total counts; see Secs. II and III [45].

The ICD counts are presented in Fig. 4(b). The atomic He^* components do not contribute to the ICD counts and are solely caused by electron impact excitation. The same is true for the electron impact ionization component, see Supplemental Material Fig. S3(c) [45]. Impact excitation of a He^* atom in a He droplet by the photoelectron mostly occurs at some distance from the He^+ photoion (see [60] and Sec. VII in [45]). In contrast, ICD produces a $\mathrm{He}^*\mathrm{He}^+$ atom-pair state at short interatomic distance given by the spacing between neighboring He atoms in droplets. This explains that ICD counts are exclusively observed for $\mathrm{He}^*\mathrm{He}^+$ molecular product states.

The relevant potential energy curves in this range are shown in Fig. 4(c). The gray arrow indicates the range of typical distances from 3.0 Å (most probable next-neighbor distance) to 3.6 Å (average He-He distance in He droplets) [58]. The decay from He^{**} to the lowest lying $2\,^2\Sigma_u^+$ and $2\,^2\Sigma_g^+$ as well as a range of higher $\mathrm{He}^*\mathrm{He}^+$ states match the resonant regions in the electron energy loss spectrum in Fig. 4(a). The large peak around 21.3 eV consists mainly of nonresonant $1s2s$ and $1s2p$-correlated

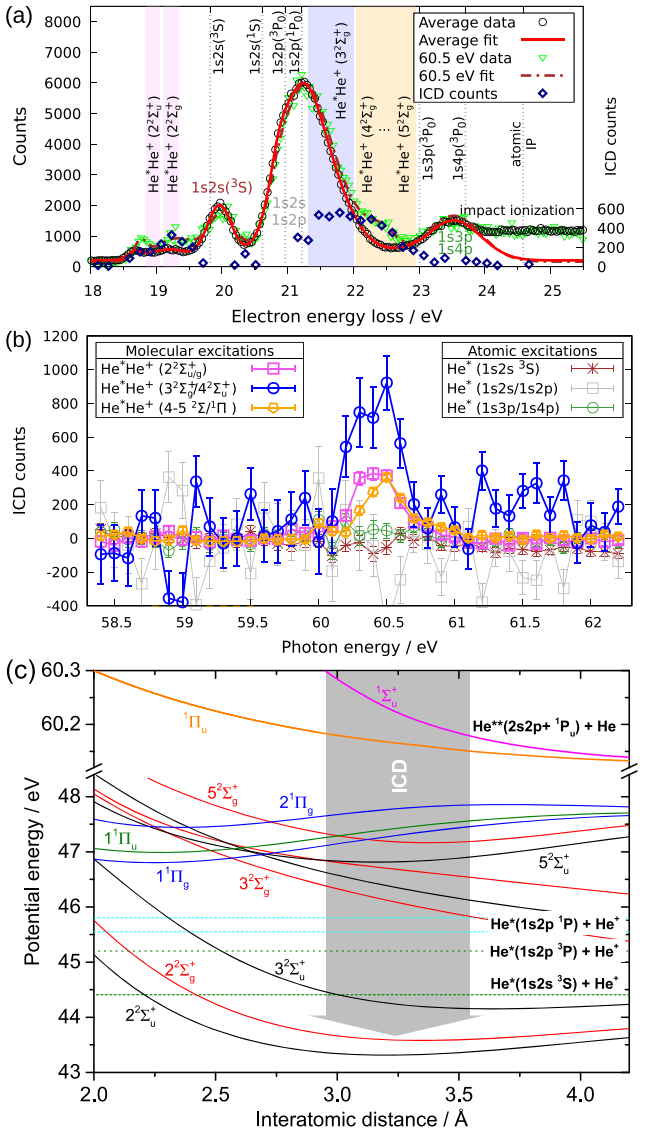

FIG. 4. (a) HEA high-resolution EEL + ICD spectrum. Black circles are averaged over 39 spectra recorded in the $h\nu = 58.4$–62.2 eV range. Green triangles show a spectrum at $h\nu = 60.5$ eV. The solid red and dash-dotted brown lines show the respective multipeak fits of a sum of 8 Gaussians. Shaded areas indicate regions where He^{**} decays by ICD into states shown in (c). Vertical dashed lines annotate atomic excitations with values from NIST [59]. (b) Photon energy dependence of the total ICD counts for excitation of different molecular and atomic excitations. (c) Potential energy curves of He_2 after double excitation of one atom and excited states of the He_2^+ molecular ion. The color encodes different symmetries as indicated by the labels. Horizontal dotted lines give the asymptotes for excitation of distant helium atoms by inelastic scattering. The gray area indicates the range of distances between neighboring He atoms in He nanodroplets where ICD takes place [58]. The potential energy curves (PECs) of $\mathrm{He}^{**}\mathrm{He}$ states were taken from Ref. [41], while the PECs of $\mathrm{He}^*\mathrm{He}^+$ states were computed using the full configuration interaction approach, as implemented in Molpro, with the aug-cc-pVDZ basis set.

atomic excitations which are shifted and broadened in droplets [60] and thus overlap with the resonant $3\,^2\Sigma_g^+$ and $4\,^2\Sigma_u^+$ components caused by ICD. The higher lying $^2\Sigma/^1\Pi$ states can energetically mix; we refrain from a more detailed assignment of states in this region due to congestions of electron spectra and the limited accuracy of the potential curves. Increasing photon energies favor higher levels of excitation (see Supplemental Material Fig. S3(d) [45]).

In conclusion, we have presented the first experimental evidence for ICD involving a doubly excited atom. ICD manifests itself as enhanced yields of He^*He^+ atom pairs and corresponding electron spectra at the Fano resonance. From the droplet-size dependence we estimate an ICD probability relative to the total ionization rate of $(3.2 \pm 0.2)\%$ in decent agreement with theoretical results. Consequently, ICD competes with AI despite the ultrashort decay time of the latter (530 vs 17.5 fs [20,21]). For higher-lying doubly excited states, the ICD probability is expected to further increase relative to AI [3]. As all atomic and molecular systems possess doubly excited states [17,18,62], this type of ICD could be relevant in other systems such as water [15] and solvated metal atoms [63,64]. In superexcited molecular systems, other ultrafast processes open up (e.g., dissociation, proton transfer), but ICD is an important relaxation channel, e.g., in water clusters and in liquid water [65,66]. Thus, ICD induced by double valence-shell excitation may present a way to site-selectively deposit energy in condensed media such as biological tissue [12,67].

We gratefully acknowledge financial support by the Danish Council for Independent Research (Grant No. 1026-00299B), the Carlsberg Foundation, the German Science Foundation (DFG) through project STI $125/19-2$, and the Danish Agency for Science, Technology, and Innovation through the instrument center DanScatt. S. R. K. gratefully acknowledges the financial support from the Ministry of Education, Government of India through the scheme for promotion of research and academic collaboration and the Institute of Eminence programmes, Government of India, and from the Max Planck Society, Germany. S. R. K., S. D., and K. S. are thankful for the support by the Indo-French Center for Promotion of Academic Research (CEFIPRA), Deutsche Akademischer Austauschdienst Dienst (DAAD), Department of Science and Technology, Government of India and the Indo-Elettra scheme. The research leading to these results has been supported by the project CALIPSOplus under Grant Agreement No. 730872 from the EU Framework Programme for Research and Innovation HORIZON 2020 and by the COST Action CA21101 "Confined Molecular Systems: From a New Generation of Materials to the Stars (COSY)." M. M. and J. D. A. thank Lars B. Madsen for fruitful discussions.

*mudrich@phys.au.dk

[1] T. Jahnke, H. Sann, T. Havermeier, K. Kreidi, C. Stuck, M. Meckel, M. Schöffler, N. Neumann, R. Wallauer, S. Voss, A. Czasch, O. Jagutzki, A. Malakzadeh, F. Afaneh, T. Weber, H. Schmidt-Böcking, and R. Dörner, Ultrafast energy transfer between water molecules, Nat. Phys. **6**, 139 (2010).

[2] M. Förstel, T. Arion, and U. Hergenhahn, Measuring the efficiency of interatomic Coulombic decay in Ne clusters, J. Electron Spectrosc. Relat. Phenom. **191**, 16 (2013).

[3] G. Jabbari, K. Gokhberg, and L. S. Cederbaum, Competition between interatomic Coulombic decay and autoionization of doubly-excited atoms, Chem. Phys. Lett. **754**, 137571 (2020).

[4] U. Hergenhahn, Interatomic and intermolecular Coulombic decay: The early years, J. Electron Spectrosc. Relat. Phenom. **184**, 78 (2011).

[5] T. Jahnke, Interatomic and intermolecular Coulombic decay: the coming of age story, J. Phys. B At. Mol. Opt. Phys. **48**, 082001 (2015).

[6] T. Jahnke, U. Hergenhahn, B. Winter, R. Dörner, U. Frühling, P. V. Demekhin, K. Gokhberg, L. S. Cederbaum, A. Ehresmann, A. Knie, and A. Dreuw, Interatomic and intermolecular Coulombic decay, Chem. Rev. **120**, 11295 (2020).

[7] L. S. Cederbaum, J. Zobeley, and F. Tarantelli, Giant intermolecular decay and fragmentation of clusters, Phys. Rev. Lett. **79**, 4778 (1997).

[8] S. D. Stoychev, A. I. Kuleff, and L. S. Cederbaum, Intermolecular Coulombic decay in small biochemically relevant hydrogen-bonded systems, J. Am. Chem. Soc. **133**, 6817 (2011).

[9] K. Gokhberg, P. Kolorenč, A. I. Kuleff, and L. S. Cederbaum, Site- and energy-selective slow-electron production through intermolecular Coulombic decay, Nature (London) **505**, 661 (2014).

[10] V. Stumpf, K. Gokhberg, and L. S. Cederbaum, The role of metal ions in X-ray-induced photochemistry, Nat. Chem. **8**, 237 (2016).

[11] X. Ren, E. Wang, A. D. Skitnevskaya, A. B. Trofimov, K. Gokhberg, and A. Dorn, Experimental evidence for ultrafast intermolecular relaxation processes in hydrated biomolecules, Nat. Phys. **14**, 1062 (2018).

[12] G. Gopakumar, I. Unger, P. Slavíček, U. Hergenhahn, G. Öhrwall, S. Malerz, D. Céolin, F. Trinter, B. Winter, I. Wilkinson, C. Caleman, E. Muchová, and O. Björneholm, Radiation damage by extensive local water ionization from two-step electron-transfer-mediated decay of solvated ions, Nat. Chem. **15**, 1408 (2023).

[13] T. Odagiri, M. Murata, M. Kato, and N. Kouchi, $(\gamma, 2\gamma)$ studies on doubly excited states of molecular hydrogen, J. Phys. B At. Mol. Opt. Phys. **37**, 3909 (2004).

[14] T. Odagiri, H. Miyagi, M. Murata, H. Fukuzawa, M. Kurokawa, M. Kitajima, and N. Kouchi, Inner-valence excited and multiply excited states of molecular oxygen around the double-ionization potential as probed by a pair of fluorescence photons, J. Phys. B At. Mol. Opt. Phys. **42**, 055101 (2009).

[15] M. Kato, T. Odagiri, K. Kodama, M. Murata, K. Kameta, and N. Kouchi, Doubly excited states of water in the inner

valence range, J. Phys. B At. Mol. Opt. Phys. **37**, 3127 (2004).
[16] L. Ishikawa, T. Odagiri, K. Yachi, T. Nakazato, M. Kurokawa, M. Kitajima, and N. Kouchi, Doubly excited states of ammonia produced by photon and electron interactions, J. Phys. B At. Mol. Opt. Phys. **41**, 195204 (2008).
[17] H. Fukuzawa, T. Odagiri, T. Nakazato, M. Murata, H. Miyagi, and N. Kouchi, Doubly excited states of methane produced by photon and electron interactions, J. Phys. B At. Mol. Opt. Phys. **38**, 565 (2005).
[18] M. E. Sandoval-Salinas and D. Casanova, The doubly excited state in singlet fission, Chem. Photon Chem. **5**, 282 (2021).
[19] U. Fano, Effects of configuration interaction on intensities and phase shifts, Phys. Rev. **124**, 1866 (1961).
[20] J. W. Cooper, U. Fano, and F. Prats, Classification of two-electron excitation levels of helium, Phys. Rev. Lett. **10**, 518 (1963).
[21] M. Domke, K. Schulz, G. Remmers, G. Kaindl, and D. Wintgen, High-resolution study of $^1p^o$ double-excitation states in helium, Phys. Rev. A **53**, 1424 (1996).
[22] J. M. Rost, K. Schulz, M. Domke, and G. Kaindl, Resonance parameters of photo doubly excited helium, J. Phys. B At. Mol. Opt. Phys. **30**, 4663 (1997).
[23] S. Barth, S. Joshi, S. Marburger, V. Ulrich, A. Lindblad, G. Öhrwall, O. Björneholm, and U. Hergenhahn, Observation of resonant interatomic Coulombic decay in Ne clusters, J. Chem. Phys. **122**, 241102 (2005).
[24] T. Aoto, K. Ito, Y. Hikosaka, E. Shigemasa, F. Penent, and P. Lablanquie, Properties of resonant interatomic Coulombic decay in Ne dimers, Phys. Rev. Lett. **97**, 243401 (2006).
[25] A. Mhamdi, F. Trinter, C. Rauch, M. Weller, J. Rist, M. Waitz, J. Siebert, D. Metz, C. Janke, G. Kastirke *et al.*, Resonant interatomic Coulombic decay in HeNe: Electron angular emission distributions, Phys. Rev. A **97**, 053407 (2018).
[26] A. Hans, F. Trinter, P. Schmidt, S. Eckart, S. Grundmann, G. Hartmann, X. Holzapfel, C. Honisch, G. Kastirke, M. Kircher *et al.*, Mechanisms of one-photon two-site double ionization after resonant inner-valence excitation in Ne clusters, Phys. Rev. Res. **5**, 013055 (2023).
[27] P. O'Keeffe, E. Ripani, P. Bolognesi, M. Coreno, M. Devetta, C. Callegari, M. Di Fraia, K. C. Prince, R. Richter, M. Alagia, A. Kivimäki, and L. Avaldi, The role of the partner atom and resonant excitation energy in interatomic Coulombic decay in rare gas dimers, J. Phys. Chem. Lett. **4**, 1797 (2013).
[28] M. Kimura, H. Fukuzawa, T. Tachibana, Y. Ito, S. Mondal, M. Okunishi, M. Schöffler, J. Williams, Y. Jiang, Y. Tamenori, N. Saito, and K. Ueda, Controlling low-energy electron emission via resonant-Auger-induced interatomic Coulombic decay, J. Phys. Chem. Lett. **4**, 1838 (2013).
[29] M. Kimura, H. Fukuzawa, K. Sakai, S. Mondal, E. Kukk, Y. Kono, S. Nagaoka, Y. Tamenori, N. Saito, and K. Ueda, Efficient site-specific low-energy electron production via interatomic Coulombic decay following resonant Auger decay in argon dimers, Phys. Rev. A **87**, 043414 (2013).
[30] F. Trinter, M. Schöffler, H.-K. Kim, F. Sturm, K. Cole, N. Neumann, A. Vredenborg, J. Williams, I. Bocharova, R. Guillemin *et al.*, Resonant Auger decay driving intermolecular Coulombic decay in molecular dimers, Nature (London) **505**, 664 (2014).
[31] A. I. Kuleff, K. Gokhberg, S. Kopelke, and L. S. Cederbaum, Ultrafast interatomic electronic decay in multiply excited clusters, Phys. Rev. Lett. **105**, 043004 (2010).
[32] A. C. LaForge, V. Stumpf, K. Gokhberg, J. von Vangerow, F. Stienkemeier, N. V. Kryzhevoi, P. O'Keeffe, A. Ciavardini, S. R. Krishnan, M. Coreno, K. C. Prince, R. Richter, R. Moshammer, T. Pfeifer, L. S. Cederbaum, and M. Mudrich, Enhanced ionization of embedded clusters by electron-transfer-mediated decay in helium nanodroplets, Phys. Rev. Lett. **116**, 203001 (2016).
[33] M. Shcherbinin, A. C. LaForge, V. Sharma, M. Devetta, R. Richter, R. Moshammer, T. Pfeifer, and M. Mudrich, Interatomic Coulombic decay in helium nanodroplets, Phys. Rev. A **96**, 013407 (2017).
[34] A. LaForge, M. Shcherbinin, F. Stienkemeier, R. Richter, R. Moshammer, T. Pfeifer, and M. Mudrich, Highly efficient double ionization of mixed alkali dimers by intermolecular Coulombic decay, Nat. Phys. **15**, 247 (2019).
[35] L. Ben Ltaief, M. Shcherbinin, S. Mandal, S. Krishnan, A. LaForge, R. Richter, S. Turchini, N. Zema, T. Pfeifer, E. Fasshauer *et al.*, Charge exchange dominates long-range interatomic Coulombic decay of excited metal-doped helium nanodroplets, J. Phys. Chem. Lett. **10**, 6904 (2019).
[36] L. B. Ltaief, M. Shcherbinin, S. Mandal, S. R. Krishnan, R. Richter, T. Pfeifer, M. Bauer, A. Ghosh, M. Mudrich, K. Gokhberg *et al.*, Electron transfer mediated decay of alkali dimers attached to He nanodroplets, Phys. Chem. Chem. Phys. **22**, 8557 (2020).
[37] Y. Ovcharenko, A. C. LaForge, B. Langbehn, O. Plekan, R. Cucini, P. Finetti, P. O'Keeffe, D. Iablonskyi, T. Nishiyama, K. Ueda, P. Piseri, M. D. Fraia, R. Richter, M. Coreno, C. Callegari, K. C. Prince, F. Stienkemeier, T. Möller, and M. Mudrich, Autoionization dynamics of helium nanodroplets resonantly excited by intense XUV laser pulses, New J. Phys. **22**, 083043 (2020).
[38] A. C. LaForge *et al.*, Ultrafast resonant interatomic Coulombic decay induced by quantum fluid dynamics, Phys. Rev. X **11**, 021011 (2021).
[39] J. D. Asmussen, R. Michiels, U. Bangert, N. Sisourat, M. Binz, L. Bruder, M. Danailov, M. Di Fraia, R. Feifel, L. Giannessi *et al.*, Time-resolved ultrafast interatomic Coulombic decay in superexcited sodium-doped helium nanodroplets, J. Phys. Chem. Lett. **13**, 4470 (2022).
[40] L. Ben Ltaief, K. Sishodia, S. Mandal, S. De, S. R. Krishnan, C. Medina, N. Pal, R. Richter, T. Fennel, and M. Mudrich, Efficient indirect interatomic Coulombic decay induced by photoelectron impact excitation in large pure helium nanodroplets, Phys. Rev. Lett. **131**, 023001 (2023).
[41] A. C. LaForge, D. Regina, G. Jabbari, K. Gokhberg, N. V. Kryzhevoi, S. R. Krishnan, M. Hess, P. O'Keeffe, A. Ciavardini, K. C. Prince, R. Richter, F. Stienkemeier, L. S. Cederbaum, T. Pfeifer, R. Moshammer, and M. Mudrich, Fano resonances observed in helium nanodroplets, Phys. Rev. A **93**, 050502(R) (2016).
[42] B. Bastian, J. D. Asmussen, L. Ben Ltaief, A. Czasch, N. C. Jones, S. V. Hoffmann, H. B. Pedersen, and M. Mudrich, A new endstation for extreme-ultraviolet spectroscopy of free

clusters and nanodroplets, Rev. Sci. Instrum. **93**, 075110 (2022).
[43] J. Tennyson, Electron-molecule collision calculations using the R-matrix method, Phys. Rep. **491**, 29 (2010).
[44] Z. Mašín, J. Benda, J. D. Gorfinkiel, A. G. Harvey, and J. Tennyson, UKRmol+: A suite for modelling electronic processes in molecules interacting with electrons, positrons and photons using the R-matrix method, Comput. Phys. Commun. **249**, 107092 (2020).
[45] See Supplemental Material at http://link.aps.org/supplemental/10.1103/PhysRevLett.132.233001 for mathematical derivations, tables, and additional figures. It includes Refs. [19,41,43,44,46–59].
[46] L. F. Gomez, E. Loginov, R. Sliter, and A. F. Vilesov, Sizes of large He droplets, J. Chem. Phys. **135**, 154201 (2011).
[47] J. P. Toennies and A. F. Vilesov, Superfluid helium droplets: A uniquely cold nanomatrix for molecules and molecular complexes, Angew. Chem., Int. Ed. Engl. **43**, 2622 (2004).
[48] H.-J. Werner, P. J. Knowles, G. Knizia, F. R. Manby, and M. Schütz, Molpro: a general-purpose quantum chemistry program package, WIREs Comput. Mol. Sci. **2**, 242 (2012).
[49] H.-J. Werner *et al.*, Molpro, version 2015.1, a package of *ab initio* programs (2015).
[50] J. Tennyson and C. J. Noble, RESON—a program for the detection and fitting of Breit-Wigner resonances, Comput. Phys. Commun. **33**, 421 (1984).
[51] D. T. Stibbe and J. Tennyson, TIMEDEL: A program for the detection and parameterization of resonances using the time-delay matrix, Comput. Phys. Commun. **114**, 236 (1998).
[52] I. V. Hertel and C.-P. Schulz, *Atoms, Molecules and Optical Physics 1. Atomic Physics and Foundations of Spectroscopy* (Springer-Verlag, Berlin, Heidelberg, 2008).
[53] J. Mezei, I. F. Schneider, and C. Jungen, Multichannel quantum defect theory of photodissociation in H_2, EPJ Web Conf. **84**, 04005 (2015).
[54] Y. Ralchenko, R. Janev, T. Kato, D. Fursa, I. Bray, and F. De Heer, Electron-impact excitation and ionization cross sections for ground state and excited helium atoms, At. Data Nucl. Data Tables **94**, 603 (2008).
[55] J. D. Asmussen, L. Ben Ltaief, K. Sishodia, A. R. Abid, B. Bastian, S. Krishnan, H. B. Pedersen, and M. Mudrich, Dopant ionization and efficiency of ion and electron ejection from helium nanodroplets, J. Chem. Phys. **159**, 034301 (2023).
[56] J. D. Asmussen, K. Sishodia, B. Bastian, A. R. Abid, L. Ben Ltaief, H. B. Pedersen, S. De, C. Medina, N. Pal, R. Richter, T. Fennel, S. Krishnan, and M. Mudrich, Electron energy loss and angular asymmetry induced by elastic scattering in superfluid helium nanodroplets, Nanoscale **15**, 14025 (2023).
[57] S. A. Chin and E. Krotscheck, Systematics of pure and doped ^{4}He clusters, Phys. Rev. B **52**, 10405 (1995).
[58] D. S. Peterka, J. H. Kim, C. C. Wang, L. Poisson, and D. M. Neumark, Photoionization dynamics in pure helium droplets, J. Phys. Chem. A **111**, 7449 (2007).
[59] A. Kramida, Y. Ralchenko, J. Reader (NIST ASD Team), NIST Atomic Spectra Database (version 5.1) (National Institute of Standards and Technology, Gaithersburg, MD) (2013).
[60] M. Shcherbinin, F. V. Westergaard, M. Hanif, S. Krishnan, A. LaForge, R. Richter, T. Pfeifer, and M. Mudrich, Inelastic scattering of photoelectrons from He nanodroplets, J. Chem. Phys. **150**, 044304 (2019).
[61] R. Flesch, N. Kosugi, A. Knop-Gericke, and E. Rühl, 2s-excitation and photoionization of neon clusters, Z. Phys. Chem. (Frankfurt/Main) **228**, 387 (2014).
[62] I. Sánchez and F. Martín, The doubly excited states of the H_2 molecule, J. Chem. Phys. **106**, 7720 (1997).
[63] P. F. O'Mahony and C. H. Greene, Doubly excited states of beryllium and magnesium, Phys. Rev. A **31**, 250 (1985).
[64] M. Baig, M. Mahmood, M. Akram, and J. Hormes, Inner-shell and double excitation spectrum of caesium involving 5p and 6s subshells, J. Phys. B At. Mol. Opt. Phys. **29**, 3871 (1996).
[65] C. Richter, D. Hollas, C.-M. Saak, M. Förstel, T. Miteva, M. Mucke, O. Björneholm, N. Sisourat, P. Slavíček, and U. Hergenhahn, Competition between proton transfer and intermolecular Coulombic decay in water, Nat. Commun. **9**, 4988 (2018).
[66] P. Zhang, C. Perry, T. T. Luu, D. Matselyukh, and H. J. Wörner, Intermolecular Coulombic decay in liquid water, Phys. Rev. Lett. **128**, 133001 (2022).
[67] V. Stumpf, K. Gokhberg, and L. S. Cederbaum, The role of metal ions in X-ray-induced photochemistry, Nat. Chem. **8**, 237 (2016).